Whale Optimization-Based PI Control for DFIG Wind Energy Systems with Modular Multilevel Grid-Side Converter

Adapa Sudheer Kumar*‡, Dondapati Ravi Kishore**, Korada Praveen Kumar***, Setty Sriram***, Peethala Vamsi***

*Department of Electrical and Electronics Engineering, Godavari Institute of Engineering and Technology (A), Rajahmundry.
**Department of Electrical and Electronics Engineering, Godavari Global University, Rajahmundry.
***Department of Electrical and Electronics Engineering, Godavari Institute of Engineering and Technology (A), Rajahmundry.
(adapasudheerk@gmail.com, dravikishore@gmail.com, koradapraveenkumar22@gmail.com, sriramsetty352@gmail.com, panduphant@gmail.com)

‡Corresponding Author: Adapa Sudheer Kumar; adapasudheerk@gmail.com

Received: 26.03.2025 Accepted:28.06.2025

Abstract - Wind energy is an effetcual and sustainable Renewable Energy Source (RES) for generating electrical power. With the global expansion of Wind Energy Conversion System (WECS), there is a growing demand for high-quality and reliable power output to ensure seamless grid integration. However, conventional control strategies face significant challenges due to the intermittent nature of wind, leading to issues such as instability, power quality degradation, and inadequate grid compliance. To conquer these challenges, this work propose a novel control framework for DFIG-based WECS using a Whale Optimization Algorithm (WOA)-tuned Proportional-Integral (PI) controller. The proposed system employs a Modular Multilevel Converter (MMC) as the grid-side converter, which ensures effective voltage regulation, harmonic reduction, and improved power quality. The Rotor-Side Converter (RSC) controls active and reactive power, while the MMC-based Grid-Side Converter (GSC) stabilizes DC-link voltage and enhances the dynamic response. The WOA-optimized PI controller dynamically adjusts control parameters, enabling better handling of wind fluctuations and grid disturbances. The proposed topology is simulated in MATLAB, demonstrate that the designed method significantly improves the system's performance by minimizing THD value of 0.62%, reducing steady-state errors, and reduced ripples.

Keywords - DFIG-based WECS, WOA-PI controller, modular multilevel converter, GSC, RSC.

1. Introduction

Concerns have recently been expressed about the depletion of non-renewable energy sources and the rise in emissions that harm the environment [1]. As a result, RESs are crucial in supplying the electrical energy requirement [2]. One essential and sustainable source of electrical power is wind energy [3]. Wind turbines are employed as important intermittent RESs in a number of nations owing to reduced energy costs and do away with fossil fuels [4]. Wind turbine power generation is a rapidly growing industry, offering a sustainable solution to reducing pollutants and carbon dioxide emissions. As more countries invest in wind power plants, the industry is poised for significant expansion, contributing to a cleaner and greener future [5]. The most popular generator type in WECSs is the Doubly Fed Induction Generator (DFIG), which has many benefits including limited speed range, partial ratings, torque and power management capabilities, decreased power converter costs, and the flexibility to run at varied speeds [6]. There are two connections on DFIG, a rotor connection that is connected via two back-to-back power converters and a stator connection that is routed straight into the grid [7]. The GSC plays a crucial role in managing power exchange between wind turbine and electrical grid [8]. The conventional GSC is typically a two-level converter connected between the DC-link and the grid, responsible for regulating voltage and controlling active and reactive power [9]. This ensures grid synchronization, power factor correction, and stability. The advantages of the conventional GSC include its ability to regulate power flow, maintain grid stability, and provide a cost-effective, proven solution for integration with the grid as shown in Fig. 1[10].

However, it has drawbacks, such as harmonic distortion, reduced efficiency at high power levels due to switching losses, limited voltage control, and scalability issues in larger systems [11]. To address these limitations, a MMC is considered in this study, offering superior voltage control, reduced harmonic distortion, and better scalability for high voltage and high power applications.

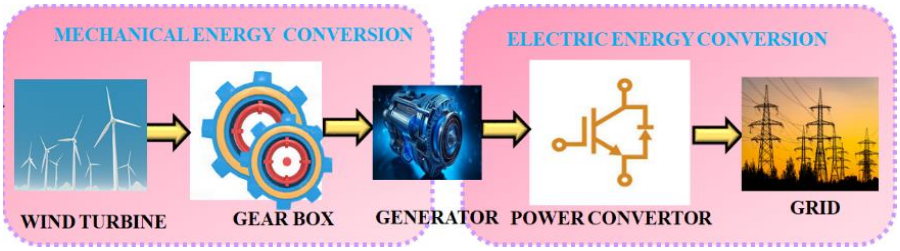


Fig. 1. Overview of DFIG based grid system.

The RSC is essential for controlling rotor currents, regulating the active and reactive power and enabling efficient variable speed operation of wind turbine [12]. The conventional approach to control the RSC typically employs PI controllers. PI controllers are widely used for their simplicity, effectiveness, and ease of implementation in maintaining the desired rotor speed and power output by adjusting the rotor-side converter's current [13]. However, tuning the parameters of PI controller is critical to ensure optimal system performance [14]. Traditional methods for tuning these parameters often rely on trial and error or analytical techniques, which may not be effective in complex, dynamic systems. To improve the performance of PI controller, optimization techniques like Genetic Algorithms (GA) [15], Particle Swarm Optimization (PSO) [16], and Artificial Bee Colony (ABC) [17] algorithms are employed. These methods are employed to automatically tune PI controller's parameters, enhancing the dynamic response, reducing oscillations and improving stability under varying wind conditions. GA and PSO are population-based optimization techniques that explore a wide search space to find the optimal solution, while the ABC algorithm mimics foraging behavior of bees to optimize controller's parameters [18-19]. The advantages of using these optimization algorithms include improved performance, faster convergence, and better adaptability to changing system dynamics compared to conventional tuning methods. However, these algorithms also have drawbacks, such as the increased computational burden, longer convergence times, and the need for fine-tuning of the optimization algorithm itself [20]. Therefore, proposed work utilized WOA-PI controller for effective control with better transient time and convergence speed. Following points shows the foremost contributions of developed topology,

- The Modular Multilevel Converter in DFIG-based grid-side converter is employed to improve power quality by reducing harmonic distortion and achieving a nearly sinusoidal output.
- DFIG-based WOA-PI based RSC is used to improve dynamic performance and system stability, achieve faster response, reduced overshoot and minimal steady-state error.

2. Proposed Methodology

The WECS utilizing a DFIG integrated with a three-phase grid through a MMC is represented in Fig. 2. The DFIG, driven by a wind turbine, converts mechanical energy into electrical power, which is regulated and controlled by two key converters such as RSC and GSC. The RSC employs Whale Optimized PI Controller to regulate the rotor's voltage and current, ensuring efficient operation by maintaining the reference voltage and active power.

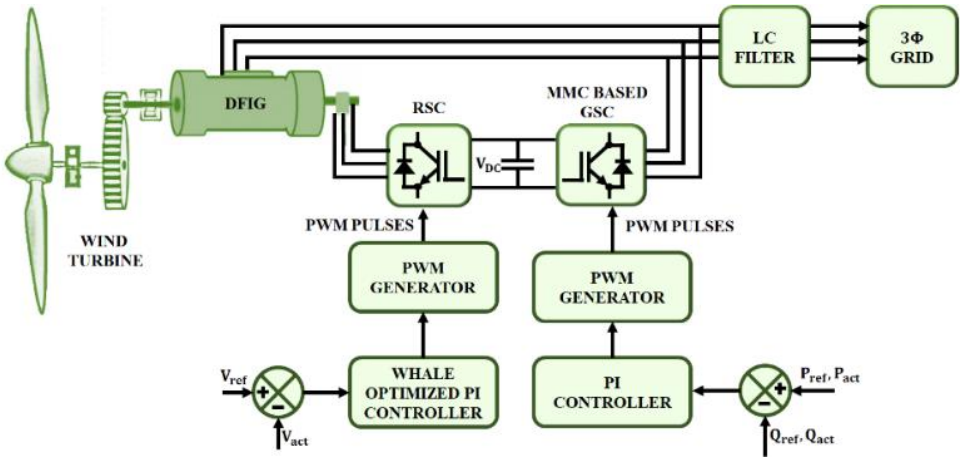


Fig. 2. Block diagram of DFIG based WECS for grid system.

On the other hand, MMC-based GSC manages power delivery to the grid while maintaining voltage stability and minimizing harmonic distortion using a PI controller. The LC filter ensures high-quality power by removing high-frequency harmonics before connecting to the grid. This configuration proves an efficient, reliable, and grid-compliant solution for wind energy systems.

2.1. Modelling of DFIG System

In Fig. 3, DFIG's equivalent circuit is displayed. The voltage and current equations for rotor and stator of DFIG in dq frame are rewritten to produce this analogous circuit. Equations [1] describe the dynamic behaviours of the DFIG's electromagnetic components are as follows:

$$v_{ds} = R_s i_{ds} - \omega_s \psi_{qs} + \frac{d\psi_{ds}}{dt} \quad (1)$$

$$v_{qs} = R_s i_{qs} - \omega_s \psi_{ds} + \frac{d\psi_{qs}}{dt} \quad (2)$$

$$v_{dr} = R_r i_{dr} - \omega_{sl} \psi_{qr} + \frac{d\psi_{dr}}{dt} \quad (3)$$

$$v_{qr} = R_r i_{dr} - \omega_{sl} \psi_{dr} + \frac{d\psi_{qr}}{dt} \quad (4)$$

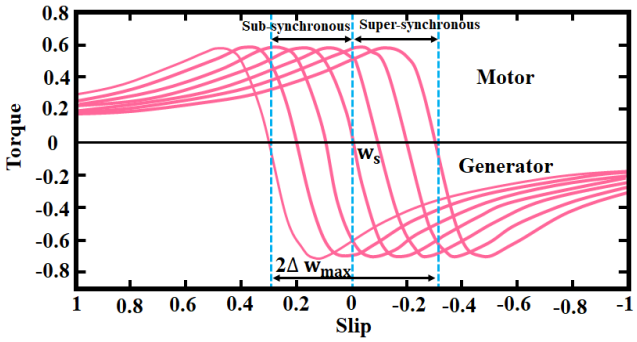


Fig. 3. Characteristics of Torque and speed in DFIG.

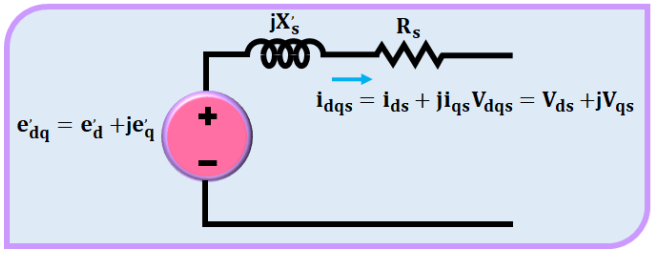


Fig. 4. Equivalent circuit of DFIG.

The Equivalent circuit is displayed in Fig. 4, The rotor and stator's magnetic flux of DFIG is derived as,

$$\psi_{dr} = L_r i_{dr} + L_m i_{ds} \quad (5)$$

$$\psi_{qr} = L_r i_{qr} + L_m i_{qs} \quad (6)$$

$$\psi_{ds} = -\left(1/\omega_s\right) e'_q + \left(X'_s/\omega_s\right) i_{ds} \quad (7)$$

$$\psi_{qs} = -\left(1/\omega_s\right) e'_d + \left(X'_s/\omega_s\right) i_{qs} \quad (8)$$

The following equation (9) expressed the electromagnetic torque and motion,

$$T_e = n_p \frac{L_m}{L_s} \left(\psi_{qs} i_{dr} - \psi_{ds} i_{qr}\right) \quad (9)$$

Here, L refer inductance, R states resistance, X states transient reactance, r and s shows rotor and stator, ψ specifies flux, d and q signified as direct and quadrature of coordinate axes, correspondingly.

2.2. Modelling of MMC

In DFIG system, MMC-based GSC is part of a back-to-back converter system, consisting of both a RSC and a GSC as outlined in Fig. 5. The MMC topology for the GSC is composed of Sub Modules (SMs) arranged in series, with each sub module consisting of a half-bridge inverter and a capacitor. The MMC architecture provides high flexibility and scalability, which is essential for large-scale wind turbine applications. Each phase of MMC contains an upper arm and lower arm, and the sub modules in the arms are interconnected through a combination of capacitors and switching devices. This allows for precise voltage control and efficient harmonic suppression when connected to the grid.

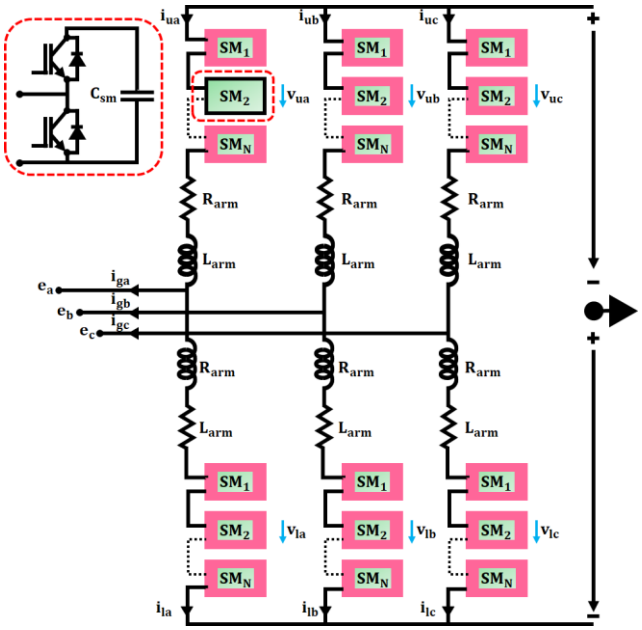


Fig. 5. Circuit of MMC converter.

The dynamic model of MMC-based GSC is described in d-q reference frame, simplifying control of active and reactive power. The grid side voltage and current are represented as:

$$i_g(t) = i_u(t) - i_l(t) \quad (10)$$

$$i_c(t) = \frac{i_u(t) + i_l(t)}{2} \quad (11)$$

Here, $i_u(t)$ and $i_l(t)$ are currents in upper and lower arms of converter, $i_g(t)$ signifies the total grid current, and $i_c(t)$ is the circulating current.

Using Kirchhoff's Voltage Law (KVL), voltage dynamics for upper and lower arms are given by,

$$L_{arm} \frac{di_u(t)}{dt} + R_{arm} i_u(t) + v_u(t) = \frac{v_{dc}}{2} \quad (12)$$

$$L_{arm} \frac{di_l(t)}{dt} + R_{arm} i_l(t) + v_l(t) = \frac{v_{dc}}{2} \quad (13)$$

Where, $v_u(t)$ and $v_l(t)$ shows he voltages over upper and lower arms, v_{dc} refers DC-link voltage and R_{arm} and L_{arm} represents are the resistance and inductance of the arm. The control of MMC-based GSC involves managing the modulation indices for the upper and lower arms, which are find based on desired grid voltage and current. The modulation indices for arms are expressed as:

$$m_u(t) = \frac{\frac{v_{dc}}{2} - v_s(t) - v_c(t)}{v_{dc}} \quad (14)$$

$$m_l(t) = \frac{\frac{v_{dc}}{2} + v_s(t) - v_c(t)}{v_{dc}} \quad (15)$$

Here, $v_s(t)$ and $v_c(t)$ represents the voltages from the phase current controller and circulating current controller. By adjusting these modulation indices, the MMC generates the desired output voltage. The modulation strategy helps to regulate the DC-link voltage at a constant level as well as ensures system is operating efficiently.

2.3. Modelling of GSC Based PI Controller

To ensure that the input currents follow reference current, PI current controllers is employed as seen in Fig. 6. In this case, input voltages to PI current controllers are as below,

$$V'_d = K_p(i_{dref} - i_d) + K_i \int (i_{dref} - i_d)dt \quad (16)$$

$$V'_q = K_p(i_{qref} - i_q) + K_i \int (i_{qref} - i_q)dt \quad (17)$$

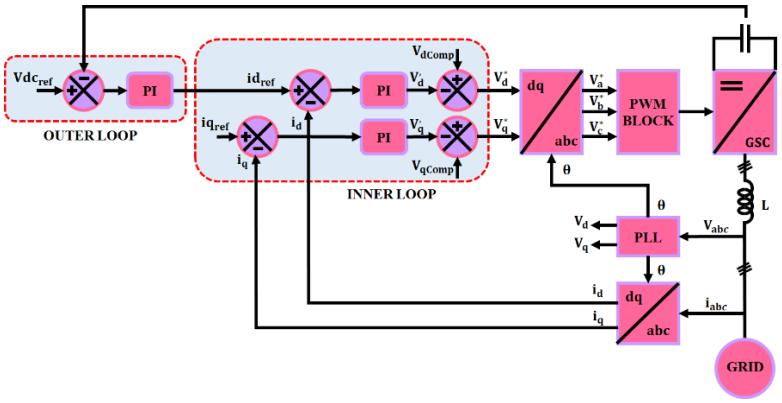


Fig. 6. Configuration of PI based GSC.

The reference voltages for d-axis and q-axis are defined as follows:

$$V_d^* = V'_d + (\omega_e L i_q + V_d) \quad (18)$$

$$V_q^* = V'_q + (\omega_e L i_d) \quad (19)$$

$$V_{dcomp} = \omega_e L i_q + V_d \quad (20)$$

$$V_{qcomp} = \omega_e L i_d \quad (21)$$

The GSC controller consists of two loops. The outer loop is reliable for controlling reference i_{dref} current, while inner loop controls and maintains a constant value for DC link voltage. The inner loop manages V_d and V_q voltages. The outer loop utilizes a PI controller to achieve its objective. In outer loop, output voltage level is scaled and compared with the given reference to calculate the error, is then fed into PI controller to determine the V'_d voltage, respectively.

2.4. Modelling of RSC Based WOA-PI Controller

The Whale Optimization Algorithm, inspired by bubble-net hunting strategy of humpback whales, has been adapted for tuning PI controllers within rotor-side control systems. This approach enhances system performance by optimally adjusting control parameters to rise the dynamic response and stability of power systems. WOA is a metaheuristic optimization method characterized by its ability to balance exploration and exploitation within the search space. The algorithm begins with an initial population of whales, each representing potential solutions. Over successive iterations, these positions are updated based on its proximity to best-known solution, the spiral-shaped movement towards prey, or random exploration for global optima. In the context of rotor-side controllers, the WOA is employed to fine-tune PI parameters by defining an objective function that minimizes deviations in critical performance metrics, such as rotor speed and voltage stability. The adaptive nature of WOA ensures precise adjustments, even under varying operating conditions.

Encircling the prey: Once the prey's location is estimated, whales adjust their positions to encircle it. Since the exact position of global optimum is unknown, the current best-known solution serves as the target prey. Whales in the swarm iteratively move closer to this solution. Over time, the position of best solution is updated, guiding other whales to refine their positions relative to this point. This behavior mimics the encircling pattern observed in real humpback whales and enables agents in WOA to navigate effectively toward optimal solutions in the search space.

The following equation (23) is expressed the movement of whale as,

$$\vec{D} = \left|\vec{C}.\overrightarrow{X^*}(t) - \vec{X}(t)\right| \quad (23)$$

$$\vec{X}(t+1) = \overrightarrow{X^*}(t) - \vec{A}.\vec{D} \quad (24)$$

Here, current iteration is expressed as t, while A *and* C are vector coefficients. The term X^* represents the best solution (or position) identified so far and X corresponds to the position vector. The operation signifies scalar multiplication between the relevant vectors. The value of $X^*$is incrementally refined in each iteration until the optimal solution is reached. The vectors A and C are expressed as below,

$$\vec{A} = 2\vec{a}.\vec{r} - \vec{a} \tag{25}$$

$$\vec{C} = 2.\vec{r} \tag{26}$$

Therefore, every search agent update their location to best places using Equation 24 and replicate the surrounding. In n-dimensional search space, the search agents swarm in hyper-cubes regarding best solution found.

2.4.1. Shrinking encircling mechanism (SEM)

In the shrinking encircling mechanism, the search space is progressively narrowed by reducing a specific parameter over iterations. This parameter controls the range of search agent's movement, allowing it to focus increasingly on the region surrounding the current best solution. The narrowing range enhances exploitation by guiding whales closer to the optimal solution while retaining some flexibility to explore nearby positions. This gradual reduction in the search range ensures precise optimization by minimizing deviation from target.

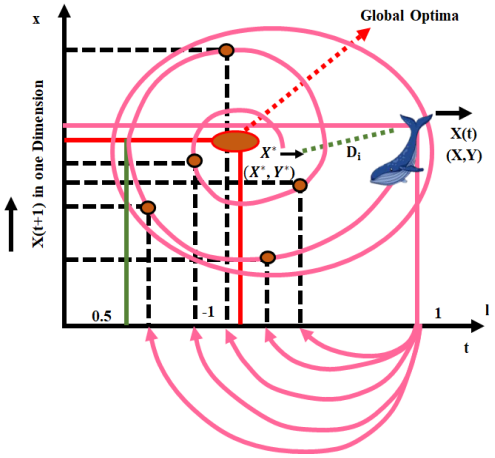


Fig. 7. Updating position of spiral mechanism.

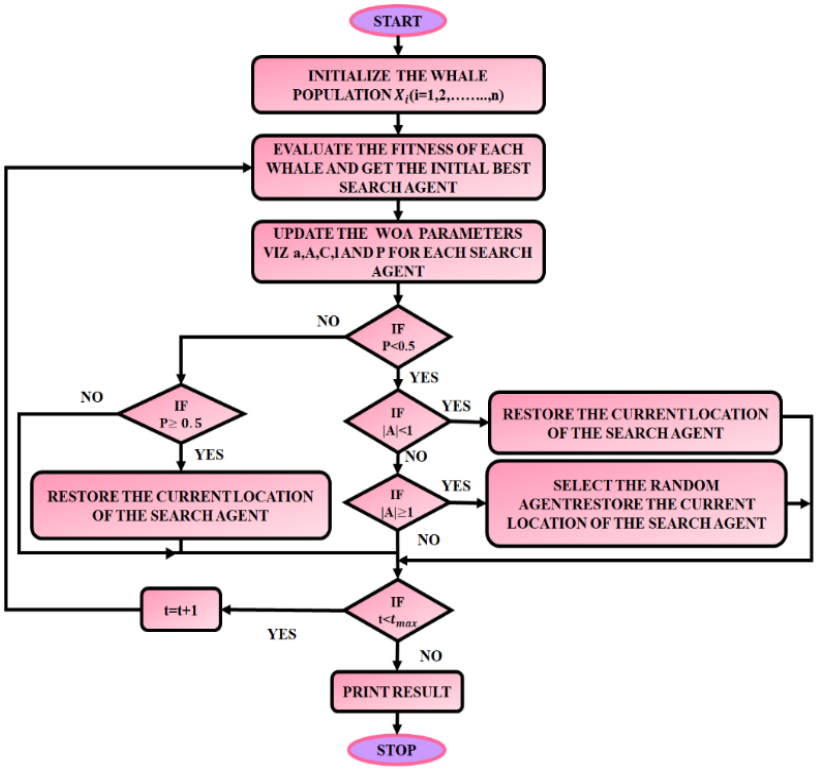


Fig. 8. Flowchart of WOA-PI controller.

2.4.2. Spiral updating position (SUP)

The spiral updating mechanism models the helical movements of humpback whales during their bubble-net hunting strategy as shown in Fig. 7. It calculates the distance between a whale's current position and the prey, then generates a spiral trajectory toward the target. This approach combines circular and spiral movements, enabling the algorithm to explore the search space effectively while maintaining focus on the prey. This mechanism is particularly useful for simulating dynamic movements in optimization problems, enhancing convergence to the global optimum.

The following Equation (27) defined the trajectory as,

$$\vec{X}(t+1) = \overrightarrow{D'}.e^{bl}.\cos(2\pi l) + \overrightarrow{X^*}(t) \qquad (27)$$

Here, $\overrightarrow{D'} = \left|\overrightarrow{X^*}(t) - \vec{X}(t)\right|$ indicates distance between ith whale and the prey (best position or solution found thus far), l ∈ [−1, 1], and b is a constant that defines geometrical slope of logarithmic spiral.

The humpback whales remarkably follow a decreasing circular spiral pattern around their prey, which ends on the prey. When updating the search agent's position during their prey-hunting journey, the spiral trajectory and the shrinking encircling trajectory are given equal weights of 50% in order to depict this hybrid trajectory simultaneously.

The numerical model for the mixed trajectory is given as below,

$$\vec{X}(t+1) = \begin{cases} \overrightarrow{X^*}(t) - \vec{A}.\vec{D} & if\ p < 0.5 \\ \overrightarrow{D'}.e^{bl}.\cos(2\pi l) + \overrightarrow{X^*}(t) & if\ p \geq 0.5 \end{cases} \qquad (28)$$

2.4.3. Random search (exploration phase)

In addition to exploiting known solutions, the WOA incorporates an exploration phase to prevent premature convergence and avoid local optima. During this phase, whales move randomly to explore a broader area of the search space. By assigning diverse values to the control parameters, the algorithm ensures robust exploration. This phase is critical for maintaining a balance over exploration and exploitation, enabling the algorithm to achieve global optimization even in complex problem domains. The overall process of proposed WOA-PI controller is illustrated in Fig. 8.

The exploration phase is numerically expressed as,

$$\vec{C} = \left|\vec{C}.\overrightarrow{X_{rand}} - \vec{X}\right| \qquad (29)$$

$$\vec{X}(t+1) = \overrightarrow{X_{rand}} - \vec{A}.\vec{D} \qquad (30)$$

Where, $\overrightarrow{X_{rand}}$ specifies an arbitrary whale with a random position vector, overall with the help of this topology, the parameters of PI controller is effectively and enhance the MMC based GSC performance.

3. Results and Discussion

This section focused the evaluation of proposed wind energy based MMC converter with optimized PI control topology from MATLAB/Simulink. The obtained outcomes are compared with the other traditional topologies for proving the proficiency of proposed topology as discussed below.

Table 1. Parameter specification for the proposed work

Parameter	Specifications
DFIG	
No. of Turbines	4
Inertia Constant	$0.685Hs$
Pairs of Poles	3
Friction Factor	0.01F(pu)
Magnetizing Inductance	2.9mH
Rotor Inductance	0.16mH(pu)
Rotor Resistance	0.016Ω (pu)
Stator Resistance	0.023 Ω (pu)
Stator Inductance	0.18mH (pu)
Frequency	50Hz
Nominal Power	10kW
MMC converter	
Input voltage	600v
Frequency	50Hz
Capacitance voltage per sub module	10mF
Switching frequency	10 Hz

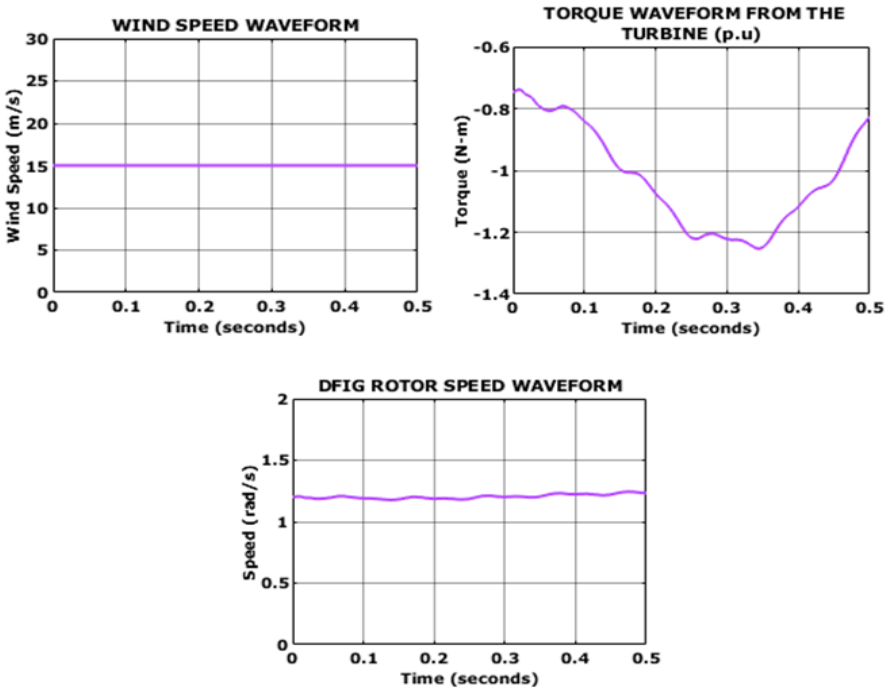


Fig. 9. Wind Speed, torque and rotor speed waveforms.

Fig. 9 illustrates the wind speed, which remains constant at approximately 15 m/s throughout the duration, indicating stable wind conditions. The turbine's torque waveform, exhibits significant fluctuations, starting around -0.8 P.U and then gradually maintain at 0.85 P.U. the rotor speed of DFIG remains relatively steady around 1.3 rad/s with minor oscillations. This stability shows effective control mechanisms, ensuring consistent performance despite torque variations.

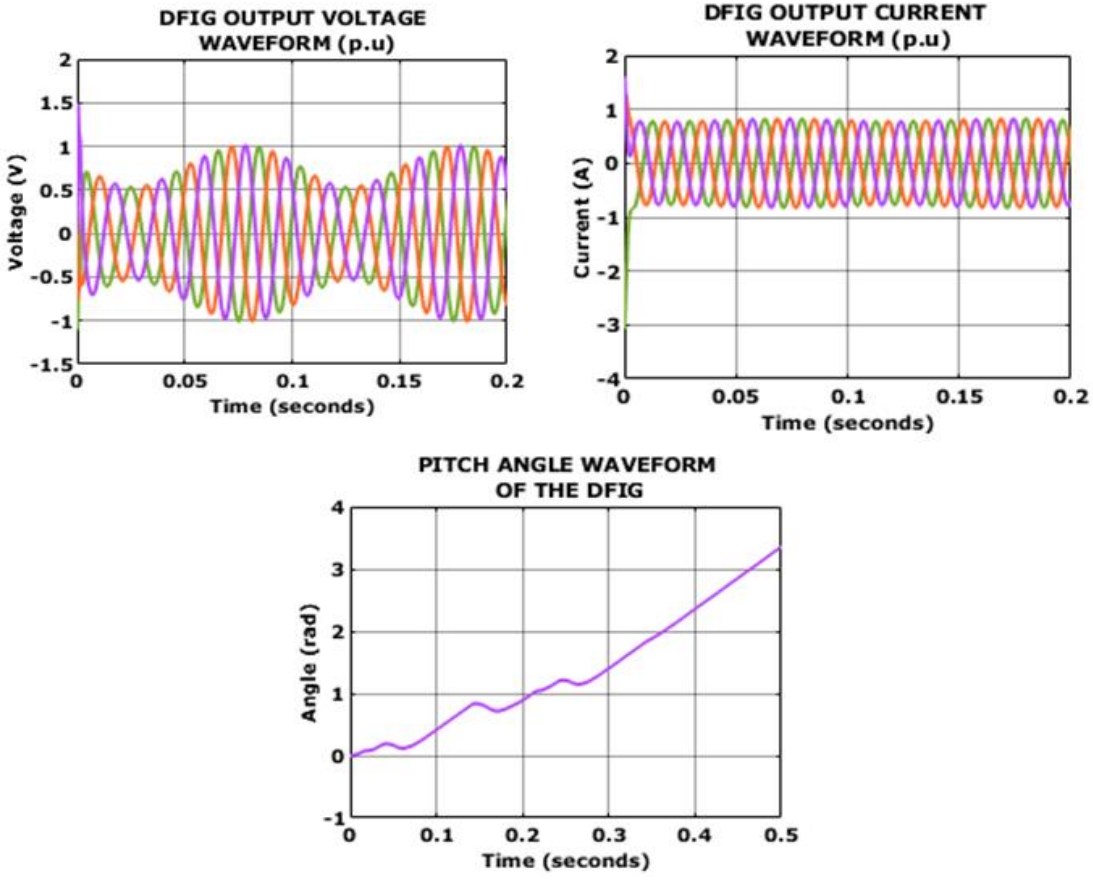


Fig. 10. DFIG output voltage, current and pitch angle waveforms.

The DFIG characteristics is illustrated in Fig. 10. It is seen that, the output voltage waveform, oscillates periodically between ±1p.u. and after 0.16s indicates stable voltage generation. Similarly, the DFIG output current waveform exhibits a sinusoidal pattern with stabilized output of ±0.8A. Moreover, the pitch angle waveform of DFIG illustrates that it highly raised and attains the stable output at 3.2rad.

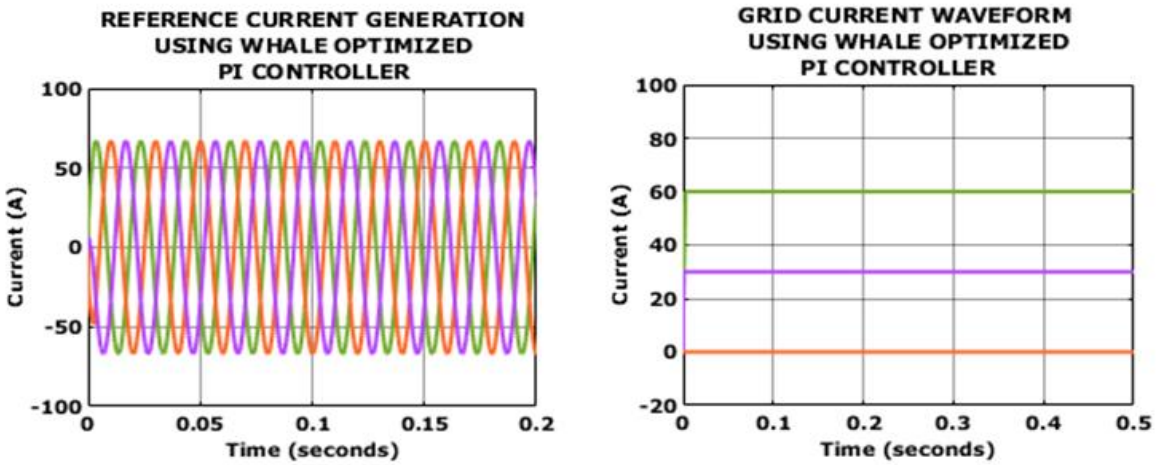


Fig. 11. Reference and grid current waveforms using WOA-PI controller.

The reference current generation using a whale-optimized PI controller, showing a steady sinusoidal waveform at 65A. Similarly, the grid current waveform controlled by the whale-optimized PI controller, which remains stable and sinusoidal with minor variations, shown in Fig. 11**.**

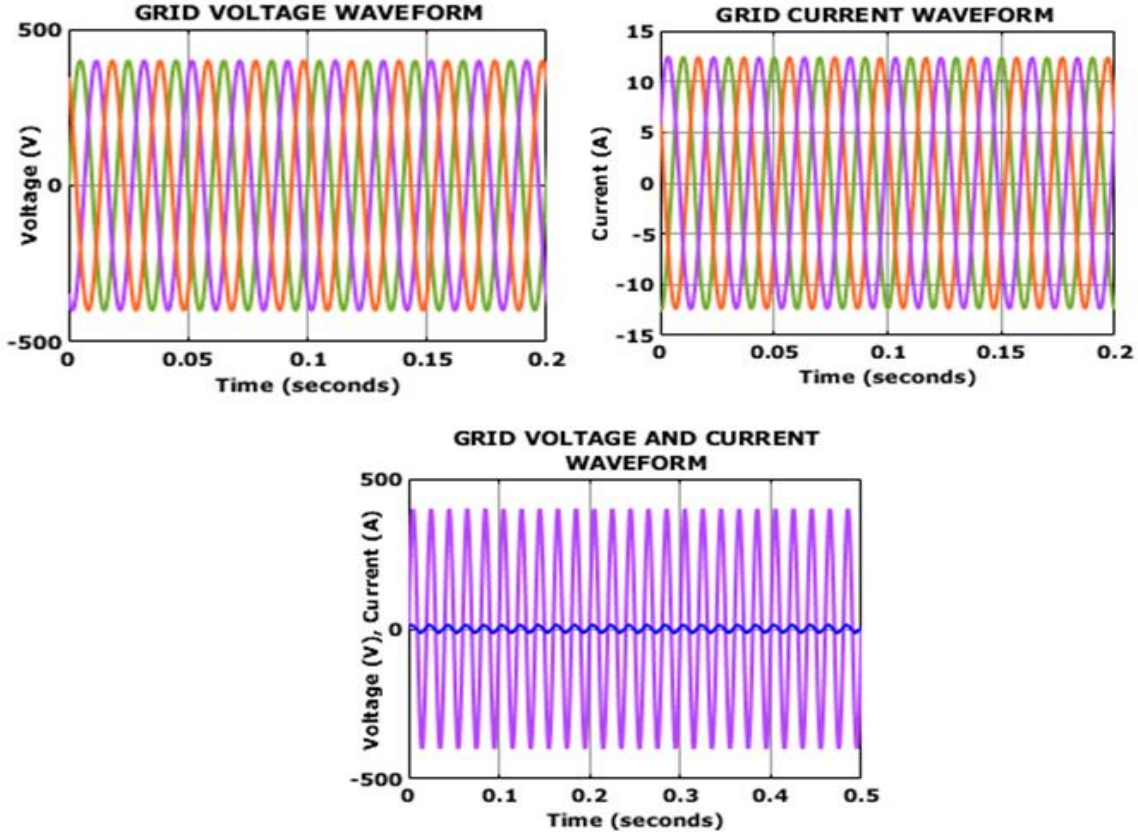


Fig. 12. Grid voltage, current and in phase waveforms.

The grid voltage waveform shows a stable sinusoidal AC voltage with a peak of approximately 415V. The grid current waveform exhibits a similar sinusoidal pattern, indicating the flow of current in sync with voltage. The combined voltage and current waveform highlights their alignment, demonstrating a typical AC power system behavior, illustrated in Fig. 12.

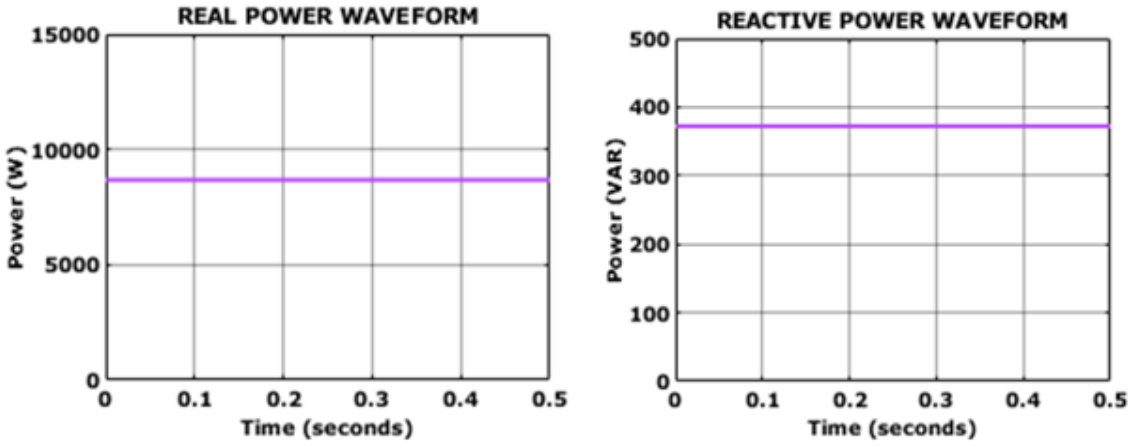


Fig. 13. Real and reactive power waveforms.

The Real Power Waveform displays in Fig. 13, shows a constant real power output, indicating stable and efficient active power delivery. The Reactive Power Waveform shows a constant value over the observed time interval of 0.5 seconds, indicating steady reactive power generation without any fluctuations.

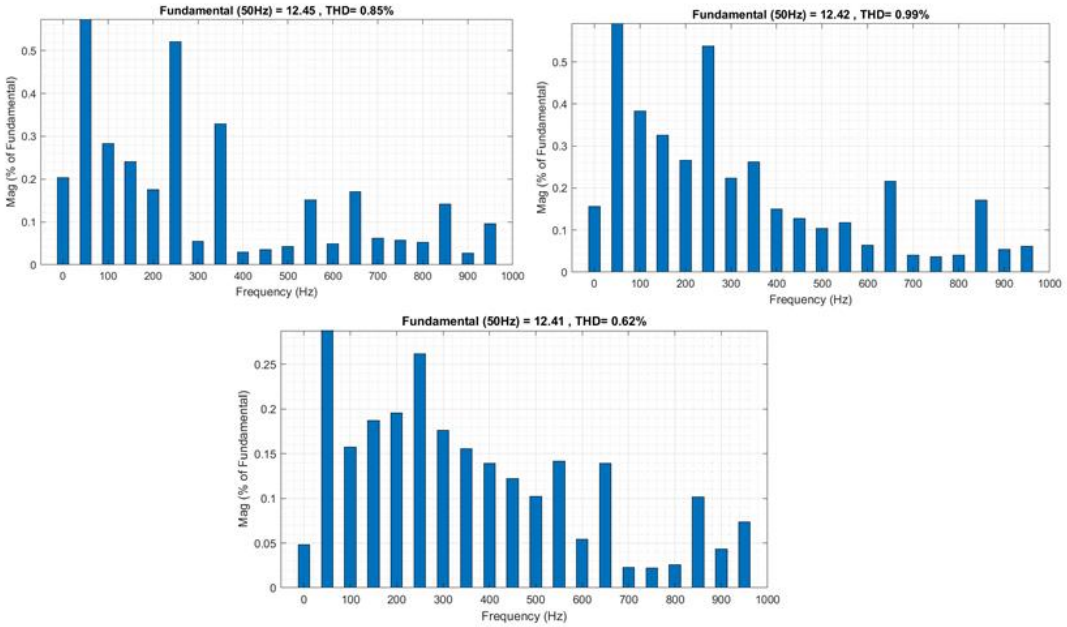


Fig. 14. THD waveforms for R, Y and B phases.

The THD waveform in Fig. 14, for the proposed topology represents the harmonic spectrum for the R, Y, and B phases. This highlights THD percentage for each phase such as in R phase, 0.85%, in Y phase 0.99% and in B phase 0.62% are accomplished, these minimized harmonics shows improved performance.

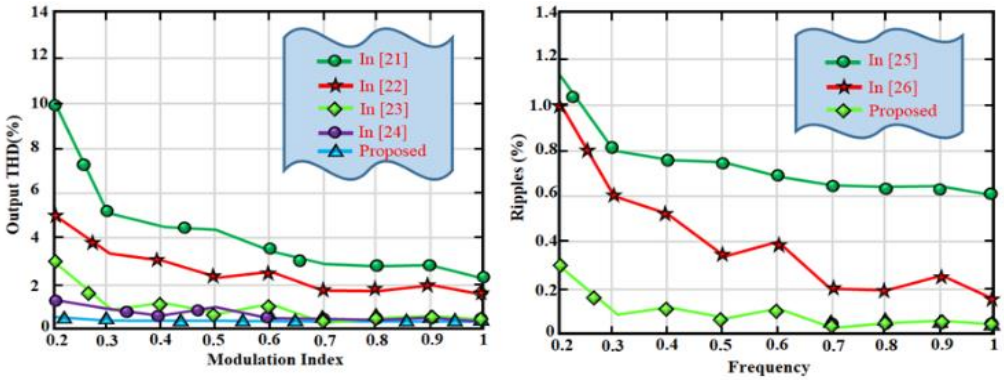


Fig. 15. Comparison of THD and ripples.

The graphs in Fig. 15 compares the effectiveness of proposed converter with other methods for THD and ripple. The first line graph illustrates the variation in THD with respect to the modulation index. The proposed converter achieves significantly lower THD of (0.62%) across the entire range of modulation indices, highlighting its optimized harmonic suppression capabilities. Also the proposed approach consistently maintains minimal ripple value of 0.29%, outperforming compared to other referenced techniques.

Table 2. Comparison of response time

Approaches	Response time (s)	Overshoot	Settling time (s)
In [27] ANN	1.2	0.03	2
In [28] cascaded fuzzy power control	1.78	0.23	1.4
In [29] PSO	0.246	0.25	0.38
Proposed	0.13	0.18	0.023

The Response time for the proposed WOA-PI controller is compared to the recently utilized approaches for showing the prominence of proposed topology. Table 2 shows that the proposed topology achieves minimized response time,overshoot and settling time of 1.12,0.18 and 0.023 with unity power factor compared to the others, which proves the effectiveness of the choosing WOA-PI controller. Additionally, proposed WOA-based PI tuning introduces only minimal computational complexity, making it suitable for real-time control applications. Despite being a metaheuristic, WOA's simple structure and low parameter dependency ensure fast convergence. Compared to traditional methods, it offers enhanced performance without significant processing overhead.

4. Conclusion

In this work, DFIG based WECS utilizing a WOA tuned PI controller is proposed for effective control. The integration of a MMC for the grid-side converter ensures superior voltage regulation, harmonic reduction, and overall power quality. The use of WOA to optimize PI controller parameters enables enhanced dynamic performance, allowing the system to effectively cope with fluctuations in wind speed and disturbances in the grid. The proposed system shows significant improvements in system stability, minimizing overshoot, THD and improving transient stability. The Simulation outcomes from MATLAB confirm that the combination of an optimized PI controller and MMC-based grid-side converter results in superior control and performance in terms of attaining minimized THD value of 0.62% with reduced ripples and response time. This approach provides a promising solution to overcome the inherent challenges of intermittent wind energy generation, contributing to the advancement of efficient and stable wind power systems for future renewable energy applications. To validate the simulation results, future work can focus on developing a real-time hardware by implementing the control scheme in an experimental setup using DSP or FPGA platforms.

References

[1] R. Dembri, L. Rahmani, B. Babes, H. G. Zaini, S. M. Ghoneim, A. K. Bojer, A. Flah and A. B. Sharaf, “SSO optimized FOFPID regulator design for performance enhancement of doubly fed induction generator based wind turbine system”, Scientific Reports, vol. 14, no. 1 28305, pp. 2024.

[2] K. Dhineshkumar, C. Subramani, G. Prakash and C. Vimala, “A modified static gain SEPIC converter renewable applications”, In AIP Conference Proceedings, vol. 2112, no. 1. AIP Publishing, 2019.

[3] H. E. Alami, B. Bossoufi, M. E. Mahfoud, M. Bouderbala, B. Majout, P. Skruch and S. Mobayen, “Robust finite control-set model predictive control for power quality enhancement of a wind system based on the DFIG generator,” Energies, vol. 16, no. 3, pp. 1422, 2023.

[4] B. Desalegn and B. Tamrat, “Overview of the PI (2DoF) algorithm in wind power system optimization and control”, Frontiers in Energy Research, vol. 12, pp. 1435455, 2024.

[5] Y. Mousavi, G. Bevan, I. B. Kucukdemiral and A. Fekih, “Active fault-tolerant fractional-order terminal sliding mode control for dfig-based wind turbines subjected to sensor faults”, In 2022 IEEE IAS Global Conference on Emerging Technologies (GlobConET), pp. 587-592. IEEE, 2022.

[6] K. Boureguig, S. Soued, F. Ouagueni and A. Chahmi, “Optimal metaheuristic-based feedback linearization control of DFIG wind turbine system”, Journal of Electrical Engineering & Technology, pp. 1-13, 2023.

[7] S. Das and B. Singh, “Enhanced control of DFIG based wind energy conversion system under unbalanced grid voltages using mixed generalized integrator”, IEEE Journal of Emerging and Selected Topics in Industrial Electronics, vol. 3, no. 2, pp. 308-320, 2022.

[8] A. A. Chhipą, P. Chakrabarti, V. Bolshev, T. Chakrabarti, G. Samarin, A. N. Vasilyev, S . Ghosh and A. Kudryavtsev, “Modeling and control strategy of wind energy conversion system with grid-connected doubly-fed induction generator”, Energies, vol. 15, no. 18, pp. 6694, 2022.

[9] I. Oraa, J. Samanes, J. Lopez and E. Gubia, “Modeling of a droop-controlled grid-connected DFIG wind turbine”, IEEE Access, vol. 10, pp. 6966-6977, 2022.

[10] H. Chojaa, A. Derouich, O. Zamzoum, A. Watil, M. Taoussi, A. Y. Abdelaziz, Z. M. Elbarbary and M. A. Mossa, “Robust control of DFIG-based WECS integrating an energy storage system with intelligent MPPT under a real wind profile”, IEEE Access, 2023.

[11] D. Ziane, B. Deffaf, S.L. Belaid, Y. Belkhier, M. Bajaj and V. Blazek, “Fuzzy Logic-Enhanced Direct Power Control for Wind Turbines with Doubly Fed Induction Generators”, Results in Engineering, pp. 103557, 2024.

[12] R. J. Vignesh, T. Senthilkumar, S. Mahendran and G. Shasikala, "Artificial Intelligence Interfaced LVRT Control for Double Fed Induction Generator Wind Energy Conversion System", 2023.

[13] A. A. Chhipą, P. Chakrabarti, V. Bolshev, T. Chakrabarti, G. Samarin, A. N. Vasilyev, S .Ghosh and A. Kudryavtsev, "Modeling and control strategy of wind energy conversion system with grid-connected doubly-fed induction generator", Energies, vol. 15, no. 18, pp. 6694, 2022.

[14] Y. Liu, D. Ćetenović, H. Li, E. Gryazina and V. Terzija, "An optimized multi-objective reactive power dispatch strategy based on improved genetic algorithm for wind power integrated systems," International Journal of Electrical Power & Energy Systems, vol. 136, pp. 107764, 2022.

[15] X. Xiang, R. Diao, S. Bernadin, S. Y Foo, F. Sun and A. S. Ogundana, "An Intelligent Parameter Identification Method of DFIG Systems Using Hybrid Particle Swarm Optimization and Reinforcement Learning", IEEE Access, vol. 12, pp. 44080-44090, 2024.

[16] Z. Liu, P. Yang, P. Zhang, X. Lin, J. Wei and N. Li, "Optimization of Fuzzy Control Parameters for Wind Farms and Battery Energy Storage Systems Based on an Enhanced Artificial Bee Colony Algorithm under Multi-Source Sensor Data", Sensors, vol. 24, no. 16, pp. 5115, 2024.

[17] M. A. Kamarposhti, H. Shokouhandeh, Y. Lee, S. K. Kang, I. Colak and E. M. Barhoumi, "Optimizing energy management in microgrids with ant colony optimization: enhancing reliability and cost efficiency for sustainable energy systems", International Journal of Low-Carbon Technologies, vol. 19, pp. 2848-2856, 2024.

[18] O. Mbah and Q. Zeeshan, "Optimizing path planning for smart vehicles: A comprehensive review of metaheuristic algorithms", J. Eng. Manag. Syst. Eng, vol. 2, no. 4, pp. 231-271, 2023.

[19] C. Maraveas, P. G. Asteris, K. G. Arvanitis, T. Bartzanas and D. Loukatos, "Application of bio and nature-inspired algorithms in agricultural engineering", Archives of Computational Methods in Engineering, vol. 30, no. 3, pp. 1979-2012, 2023.

[20] G. Devika and A. G. Karegowda, "Bio-inspired optimization: algorithm, analysis and scope of application", In Swarm Intelligence-Recent Advances and Current Applications, IntechOpen, 2023.

[21] M. Kurtoğlu and A. M. Vural, "A novel nearest level modulation method with increased output voltage quality for modular multilevel converter topology", International Transactions on Electrical Energy Systems, vol. 2022, no. 1, pp. 2169357, 2022.

[22] V. T. Nguyen, J. W. Kim, J. W. Park, J. M. Lee and B. G. Park, "A modified submodule of modular multilevel converter using active power decoupling method for reducing capacitor voltage ripple under low-frequency operation", IET Power Electronics, vol. 16, no. 5, pp. 868-882, 2023.

[23] S. Haq, S. P. Biswas, M. K. Hosain, M. A. Rahman, M. R. Islam and S. Jahan, "A modular multilevel converter with an advanced PWM control technique for grid-tied photovoltaic system", Energies, vol. 14, no. 2, pp. 331, 2021.

[24] A. A. Hafez, A. A. Mahmoud and A. M. Yousef, "Robust and intelligent control for single-stage grid-connected modular multilevel converter in PV applications", Journal of Electrical Engineering & Technology, vol. 16, pp. 917-931, 2021.

[25] S. Wang, D. Bao, G. Gontijo, S. Chaudhary and R. Teodorescu, "Modeling and mitigation control of the submodule-capacitor voltage ripple of a modular multilevel converter under unbalanced grid conditions", Energies, vol. 14, no. 3, pp. 651, 2021.

[26] G. Gontijo, S. Wang, T. Kerekes and R. Teodorescu, "Performance analysis of modular multilevel converter and modular multilevel series converter under variable-frequency operation regarding submodule-capacitor voltage ripple", Energies, vol. 14, no. 3, pp. 776, 2021.

[27] A. Elnozahy, A. M. Yousef, F. K. Abo-Elyousr, M. Mohamed and S. A. Abdelwahab, "Performance improvement of hybrid renewable energy sources connected to the grid using artificial neural network and sliding mode control", Journal of Power Electronics, vol. 21, pp. 1166-1179, 2021.

[28] H. Benbouhenni, I. Colak, N. Bizon, M. I. Mosaad and T. G. Tella, "Power regulation of variable speed multi rotor wind systems using fuzzy cascaded control", Scientific Reports, vol.14, no. 1, pp. 16415, 2024.

[29] S. Kumar, A. Gupta and R. K. Bindal, "Load-frequency and voltage control for power quality enhancement in a SPV/Wind utility-tied system using GA & PSO optimization", Results in Control and Optimization, vol. 16, pp.100442, 2024.